Direct capture of low-concentration CO_2 and selective hydrogenation to CH_4 over Al_2O_3-supported Ni-La dual functional materials

Journal:	*Green Chemistry*
Manuscript ID	GC-ART-07-2024-003218
Article Type:	Paper
Date Submitted by the Author:	02-Jul-2024
Complete List of Authors:	Tatsumichi, Tomotaka; Kogakuin University Okuno, Rei; Kogakuin University Hashimoto, Hideki; Kogakuin University, Department of Applied Chemictry Namiki, Norikazu; Kogakuin University - Hachioji Campus Maeno, Zen; Kogakuin University

Direct capture of low-concentration CO_2 and selective hydrogenation to CH_4 over Al_2O_3-supported Ni-La dual functional materials

Tomotaka Tatsumichi[a], Rei Okuno[a], Hideki Hashimoto[a,b], Norikazu Namiki[a], Zen Maeno[a,*]

[a]School of Advanced Engineering, Kogakuin University, 2665-1, Nakano-machi, Hachioji, Tokyo, 192-0015, Japan
[b]Center for Basic Research on Materials, National Institute for Materials, Science, 1-2-1, Sengen, Tsukuba, Ibaraki 305-0047, Japan, PRESTO, Japan Science and Technology Agency (JST), Kawaguchi, Saitama, 332-0012, Japan

*Corresponding author
Zen Maeno, E-mail: zmaeno@cc.kogakuin.ac.jp

Abstract

CO_2 capture and reduction with H_2 (CCR) to synthesise CH_4 over dual-functional materials (DFMs) possessing CO_2 capture and hydrogenation abilities has recently attracted attention as a promising methodology for utilising low-concentration CO_2 in air or exhaust gases without pressure and/or temperature swing operations. Much effort has been devoted to the development of Ni-based DFMs for the CCR of CH_4 formation owing to their low cost and high catalytic potential for Ni methanation. However, previous studies have been investigated under relatively high reaction temperatures (400–600 °C) and/or pressurised H_2 conditions. In addition, experiments were conducted in the absence of O_2 in the simulated CO_2 gas. The development of efficient Ni-based DFMs under milder and more realistic reaction conditions is still necessary. In this study, we developed La-modified Al_2O_3-supported Ni nanoparticles (Ni-La(X)/Al_2O_3, X denotes the La loading) for the selective formation of CH_4 from low-concentration CO_2 (1%) in a simulated gas containing O_2 (20%). The optimised Ni-La(15)/Al_2O_3 showed 98% selectivity for CH_4 formation under isothermal (350 °C) and non-pressurised conditions. The effect of the La loading amount on the CCR performance was studied using X-ray diffraction, temperature-programmed surface reactions, and steady-state CO_2 hydrogenation. Furthermore, the developed Ni-La(15)/Al_2O_3 was applied to direct capture of ultralow concentration CO_2 in air (ambient direct air capture (DAC)) and methanation.

Introduction

To reduce CO_2 emissions and establish a carbon-neutral society, demands for developing new technology for CO_2 capture and utilization are increasing. CO_2 adsorption and desorption using liquid and solid adsorbers, including amine- and zeolite-based materials, have been extensively studied.[1–7] These systems are based on pressure and/or temperature swing operations, which are energy-intensive processes requiring large-scale plants. Their target concentration was >10%, limiting their applicability in capturing low-concentration CO_2. As an alternative strategy, CO_2 capture and reduction with H_2 (CCR) has recently attracted significant attention.[8–25] Low-concentration CO_2 and H_2 gases alternately flow in reactor systems during unsteady-state operations, where the captured CO_2 is converted to CH_4 and CO. CO_2 adsorbers and CO_2 hydrogenation catalysts were combined regardless of the reactor type. In these cases, the operating temperatures often differ between CO_2 capture and hydrogenation. Dual-functional materials (DFMs) with CO_2 capture and hydrogenation abilities have recently attracted considerable attention because they enable isothermal CCR operation. Alkaline (earth) metal oxides/carbonates are co-loaded onto metal oxide supports with transition metal species, mainly group 8-10 metals. The concept and protocol have been first reported by Urakawa et al. and Farrauto et al., independently.[15,25] For CH_4 synthesis, Farrauto et al. developed Ru and Ca co-loaded Al_2O_3 for CCR under isothermal conditions of 320 °C.[15] Ru-based DFMs were also investigated by several research groups.[10–13,20] In addition, Ni-based DFMs were explored because of their low cost and ubiquity[17,21,23,24,26] The reported Ni-Ca-based DFMs suffer from lower activity owing to the low reducibility of the Ni oxide species[23]. To perform the CCR in the temperature range below 400 °C, O_2-free simulated CO_2 gas was often utilised.[17,24] Toward the application for O_2-containing low-concentration CO_2 gas, the group of Kuramoto and Urakawa studied the CCR over Ni-based DFMs under higher reaction temperature conditions of 450 °C where Na-loaded Al_2O_3-supported Ni (Ni-Na/Al_2O_3) was the most effective.[21] However, the reported Ni-Na/Al_2O_3 still has limitations, such as using pressurized H_2 gas to obtain high CH_4 selectivity. Recently, Ni-K/Al_2O_3 was developed as an efficient Ni-based DFM under low-temperature conditions, in which selective CH_4 formation was not achieved[27]. The development of Ni-based DFMs for selective CH_4 synthesis via CCR under mild reaction conditions is still essential.

La-loaded Al_2O_3 is an effective support for promoting catalytic reactions over metal nanoparticles.[28–31] Liu et al. reported that La co-loading improved the catalytic activity of Al_2O_3-supported Ni nanoparticles (Ni/Al_2O_3) during steady-state CO hydrogenation.[32] In steady-state CO_2 hydrogenation, La-co-loaded Ni/Al_2O_3 showed higher activity and selectivity for CH_4 formation, where the co-loaded La reserved CO_2 on the catalyst surface by chemisorption.[29] Ni and La co-loaded Al_2O_3 has a potential to be effective DFMs for CCR operation.

In this study, we aimed to investigate the CCR performance of Ni-La/Al_2O_3 using O_2-containing low-concentration CO_2 and atmospheric-pressure H_2 gases under the isothermal conditions of 350 °C. Ni-La/Al_2O_3 exhibited high CH_4 selectivity for the hydrogenation of captured CO_2. The optimum La loading was 15 wt.%, and the selectivity for CH_4 formation was 98%. This value was better than those obtained by the Ni-Na and Ni-Ca/Al_2O_3 prepared under similar conditions. The developed Ni-La/Al_2O_3 was applied to ambient direct air capture (DAC) to successive methanation.

Experimental

Catalyst preparation

Al_2O_3 (gamma-Al_2O_3, PURALOX SBa 200) was supplied by SASOL Ltd. La was added to an Al_2O_3 support by impregnation. An aqueous solution containing $La(NO_3)_3$ was impregnated onto the Al_2O_3 support, where the amounts of $La(NO_3)_3·6H_2O$ and Al_2O_3 were varied to change the La loading amount (see below). The mixture was evaporated at 50 °C, dried at 90 °C overnight, and calcined in air at 600 °C for 2 h to yield La(X)/Al_2O_3 (X denotes the La loading amount, X = 5, 15, 30, and 50 [wt%]). Ni-La(X)/Al_2O_3 (X = 5, 15, 30, and 50 wt %) and Ni/Al_2O_3 were prepared similarly using an impregnation method. 0.9 g of La(X)/Al_2O_3 or Al_2O_3 was added to 50 mL of an aqueous solution that contains 0.49 g of $Ni(NO_3)_2·6H_2O$, corresponding to 10 wt% of Ni. The mixture was evaporated, dried, and calcined in air at 500 °C (2 h). Ni-Na/Al_2O_3 and Ni-Ca/Al_2O_3 were similarly prepared, with Na and Ca loadings of 3 and 4 wt%, respectively. Unless otherwise noted, the samples were used for various characterization experiments without pretreatment.

Characterization

X-ray diffraction (XRD) was performed using Cu-Kα radiation on a Rigaku MiniFlex600. An AUTOSORB 6AG (Yuasa Ionics Co.) was used for N_2 adsorption measurements to determine the specific surface areas. High-angle annular dark-field scanning transmission electron microscopy (HAADF-STEM) images were recorded using an FEI Titan G2 microscope with an EDX analyzer whereas TEM images were obtained using an JEM-2100.

^{27}Al magic angle spinning (MAS) and nuclear magnetic resonance (NMR) spectroscopy of the as-prepared and heated samples were performed using a JEOL JNM-ECZ800R (18.79 T) spectrometer at a ^{27}Al Larmor frequency of 208.45 MHz. The samples were packed in zirconia rotors and spun at 20 kHz using a 3.2 mm HXMAS probe. The ^{27}Al chemical shift δ_{iso} in parts per million (ppm) was referenced to an external 1 mol dm^{-3} $AlCl_3$ solution (−0.1 ppm). X-ray absorption spectroscopy (XAS) was performed using BL14B2 in SPring-8. X-ray absorption near edge structure (XANES) spectra were analyzed using the Athena software ver. 0.9.25, which is included in the Demeter package[33].

CO_2 capture and reduction with H_2 (CCR)

The experimental procedure consisted of a gas supply system, timer-controlled four-way valve, electronic furnace, and Fourier-transform infrared (FTIR) spectroscopy for gas detection. The four-way valve was connected to two gas lines for the simulated CO_2 gas, including CO_2, O_2, N_2, and H_2. 0.1 g of DFMs were heated to 350 °C for 15 min under N_2 flow. After H_2 pretreatment was performed under 100 mL/min of 20% H_2/N_2 flow for 30 min, the CCR test was conducted by alternating the gas flows for CO_2 capture (100 mL/min of 1% CO_2+20% O_2/N_2) and reduction (100 mL/min of 20% H_2/N_2) for each 5 min. Maximum CH_4 concentration (C_{CH4_max}) was determined at the top of the CH_4 production peak. Equations (1)-(4) were used to calculate the amount of CO_2 adsorption (Ad_{CO2}) and CH_4 formation (Q_{CH4}), CH_4 selectivity, and conversion of captured CO_2 where W, t, and F_m (m = CO_2, CH_4, or CO) denote the catalyst weight, time, and molar flow rate, respectively.

$$Ad_{CO2}[mmol\,/g] = \frac{1}{W}\int_{t_{CO_2,\,start}}^{t_{CO_2,\,end}} (F_{CO2,in}(t) - F_{CO2,out}(t))dt \quad . . (1)$$

$$Q_{CH4}[\mathrm{mmol/g}] = \frac{1}{W}\int_{t_{H_2,\,start}}^{t_{H_2,\,end}} F_{CH4}(t)dt \quad . . . (2)$$

$$S_{CH4} = \frac{Q_{CH4}}{Q_{CH4} + Q_{CO}} \quad . . . (3)$$

$$Conv_{adCO2} = \frac{Q_{CH4} + Q_{CO}}{Ad_{CO2}} \quad . . . (4)$$

Note that the response of CO_2 with SiC as an inert material was similar to that in the blank test (Figure S1). For application of DAC to methane as well as effect of vapor co-feeding, 2 g of Ni-La(15)/Al_2O_3 was put in the middle of a quartz tube (i.d. 10 mm), and both sides were filled with quartz balls (ϕ 5 mm) so that the dead space considerably decreased. Ambient air (500 mL/min) containing ~400–500 ppm CO_2 was allowed to flow for 3 min (DAC) followed by purge with N_2 flow (500 mL/min for 3 min). Then, 100 mL/min of H_2 was flowed to hydrogenate captured CO_2 for 3 min, After the purge with N_2 for 3 min, ambient air was flowed again to repeat DAC and methanation. The above gas-switching process was repeated for 80 cycles. The compressed air was used without dehumidification. The generated CH_4 and CO were monitored by FTIR combined with gas cell (approximately 60 mL) whereas the concentration of uncaptured CO_2 in effluent gas was recorded by a CO_2 recorder (TR-76Ui-S, T&D cooperation) in a chamber (approximately 2 L) (Figure S2). Note that the kinetic curve of CO_2 concentration in DAC and methanation was low responsibleness because of the relatively large volume of chamber.

Results and discussion

CCR performance of Ni-La/Al_2O_3 and other Ni-based DFMs

The simulated CO_2 gas and H_2 were alternatively flowed into the reactor containing 100 mg of DFMs at 350 °C. The results are summarized in Table 1. Before the CCR test, the DFMs were pretreated with 100 mL/min of 20% H_2/N_2 for 30 min. Ni/Al_2O_3 without La co-loading showed low Q_{CH4} and C_{Max} (0.023 mmol/g and 517 ppm, respectively). By contrast, Ni-La(15)/Al_2O_3 exhibited higher Q_{CH4} and C_{Max} values (0.124 mmol/g and 6200 ppm, respectively). The amount of CO_2 capture (Ad_{CO2}) was also enhanced from 0.049 to 0.129 mmol/g, indicating that the co-loaded La species provided effective CO_2 capture sites. Notably, CO was barely detected in the effluent gas during hydrogenation (Figure 1a), and the S_{CH4} value was 98%. A series of Ni-La(X)/Al_2O_3 samples were prepared, and the effects of the La loading on Q_{CH4} and C_{Max} were studied. The Q_{CH4} value increased from 0.030 to 0.129 mmol/g with the increase of loading amount from 5 to 15 wt% (Figure 2). Although the further increase from 15 to 30 wt% slightly enhanced Q_{CH4} to 0.156 mmol/g, the Q_{CH4} value was much lower (0.067 mmol/g) at 50 wt% (Figure 1b). Regarding the C_{CH4_Max} value (Figure 2), a volcano-type dependency was obtained, and the highest value (6200 ppm) was obtained at 15 wt%. Considering the CCR operation with a short interval time, 15 wt% was the best loading amount. The conversion value based on the amounts of CO_2 capture and CH_4/CO formation was determiend as 97%, showing that almost of capture CO_2 was converted to CH_4. The use of La(15)/Al_2O_3 without Ni loading resulted in low Q_{CH4} and C_{Max}

(0.020 mmol/g and 146 ppm, respectively), demonstrating that co-loading of Ni and La are essential to promote CO_2 capture and hydrogenation efficiently.

Table 1 Results of CCR test over a series of Ni-based DFMs

DFM	Ad_{CO2} [a] [mmol/g]	Q_{CH4} [a] [mmol/g]	C_{CH4_Max} [b] [ppm]	S_{CH4} [c] [%]	$Conv_{adCO2}$ [c] [%]
Ni/Al_2O_3	0.049	0.032	820	96	68
Ni-La(15)/Al_2O_3	0.129	0.124	4888	99	97
Ni-Ca(4)/Al_2O_3	0.118	0.118	4177	99	99
Ni-Na(3)/Al_2O_3	0.161	0.144	5180	89	99

Reaction conditions: 0.1 g of catalyst, 350 °C, 100 mL/min of 1% CO_2+20% O_2/N_2 for 5 min, followed by 100 mL/min 20% H_2 /N_2 for 5 min. b Composition of the effluent gas at the outlet was quantitatively analysed using FTIR spectroscopy combined with a gas cell. c Based on the amount of CO and CH_4 generated during the reduction period.

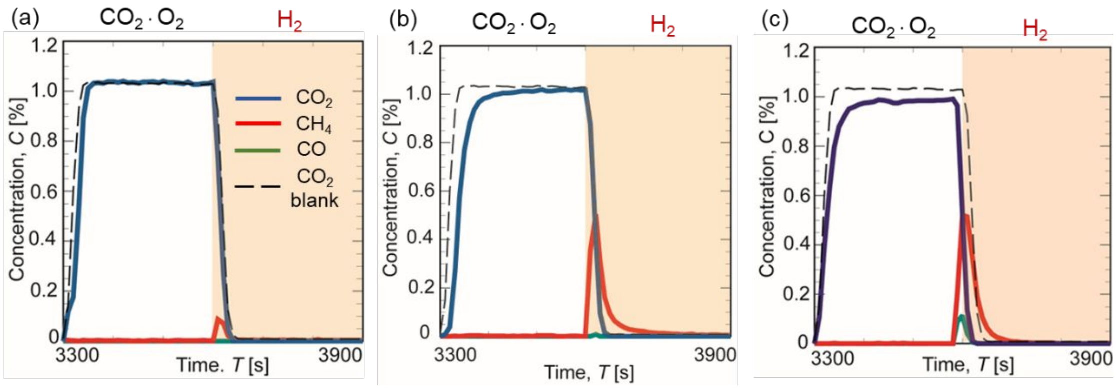

Figure 1. Concentration profile of CO_2, CH_4, and CO in CO_2 capture in the presence of O_2 and hydrogenation using (a) Ni-La(15)/Al_2O_3, (b) Ni-La(50)/Al_2O_3, and (c) Ni-Na(3)/Al_2O_3. Reaction conditions: 100 mg of Ni-based DFM, CO_2 capture under simulated gas containing O_2 (100 mL/min of 1% CO_2+20% O_2/N_2) for 5 min and successive hydrogenation (100 mL/min of 20% H_2/N_2 for 5 min) using Ni-based DFMs.

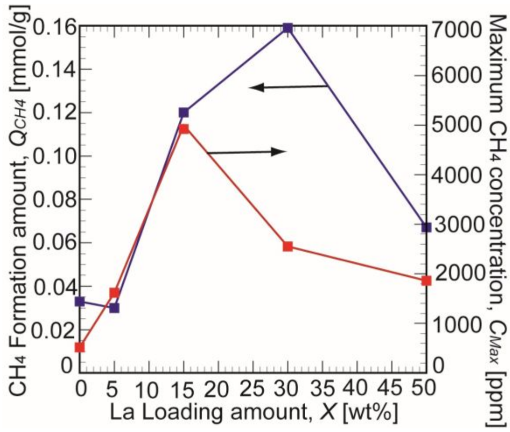

Figure 2. Effect of La loading amount on formation amount and maximum concentration of CH_4 in CCR using Ni-La(*X*)Al_2O_3.

The optimized Ni-La(15)/Al_2O_3 was further compared with Na- or Ca-co-loaded Ni/Al_2O_3, Ni-Na(3)/Al_2O_3 and Ni-Ca(4)/Al_2O_3 with similar molar loading amount (1.0 to 1.3 mmol/g). The results are summarized in Figure 3a-c. The use of Ni-Na(3)/Al_2O_3 decreased the S_{CH4} value to 89%, although the Q_{CH4} and C_{Max} values were higher than those for Ni-La(15)/Al_2O_3 (0.144 mmol/g and 7624 ppm, respectively). When Ni-Ca(4)/Al_2O_3 was used, the Q_{CH4} and C_{Max} were slightly lower (0.118 mmol/g and 4170 ppm, respectively) while the high CH_4 selectivity was obtained. The influence of coexisting O_2 in the simulated CO_2 gas was also tested. Ni-La(15)/Al_2O_3 exhibited a similar Q_{CH4} regardless of the presence or absence of O_2 (0.124 and 0.120 mmol/g), which is in sharp contrast to the results obtained using Ni-Na(3)/Al_2O_3, where Q_{CH4} significantly decreased from 0.173 to 0.144 mmol/g (Table S1). Ni-La(15)/Al_2O_3 is an effective DFM for the CCR to selective CH_4 formation under milder reaction conditions. Although the CCR performance of our Ni-La(15)/Al_2O_3 was lower than that for Ru-based DFMs, our DFM is comparable or superior to the state-of-the-art Ni-based ones under milder and more realistic conditions (Table S2). A possible reason for better O_2-resistance of Ni-La(15)/Al_2O_3 was ascribed to the oxidized state of Ni species even in H_2 flow at CCR operation temperature (vide infra). The good CCR performance of Ni-La(15)/Al_2O_3 was maintained in multiple cycles even in the co-presence of O_2 (Figure S3).

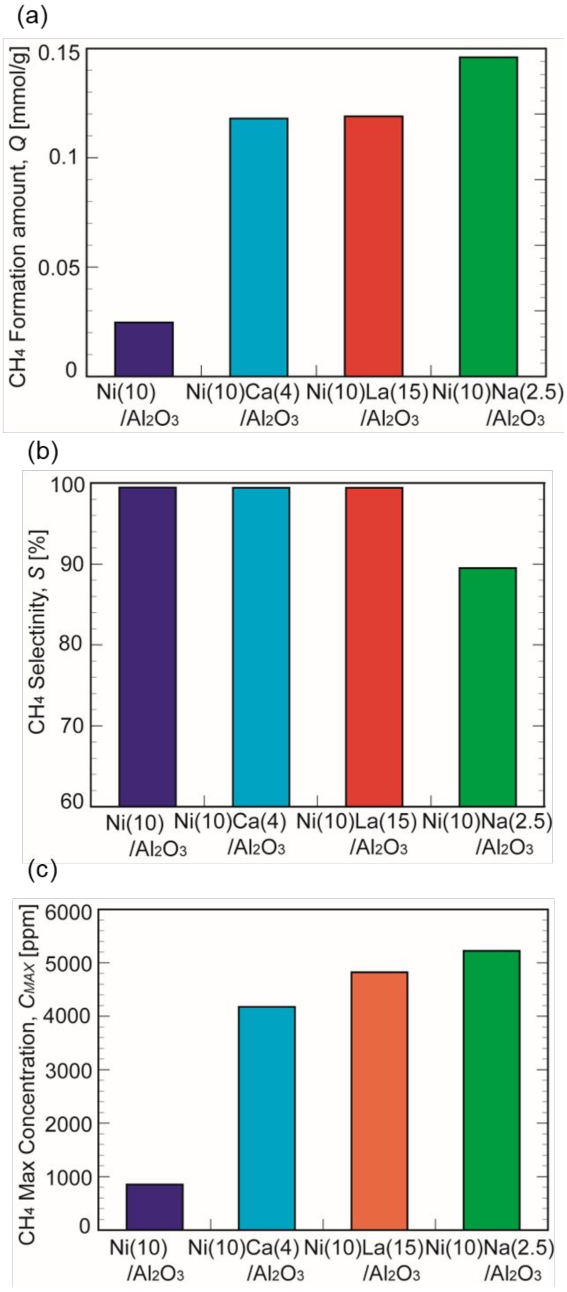

Figure 3 Comparison of CCR performance, (a) Q_{CH4}, (b) S_{CH4}, and (c) C_{Max}, of Ni-based DFMs with different co-loaded metals (Ca, La, and Na).

Characterization of Ni-La/Al_2O_3

The specific surface areas of La(*X*)/Al_2O_3 and Ni-La(*X*)/Al_2O_3 were determined by N_2 adsorption. La loading resulted in a decrease in the surface area, which monotonically decreased from 178 to 50 m^2/g with an increase in the loading amount from 5 to 50 wt% (Figure 4). A similar trend was reported for La-loaded Al_2O_3-supported metal nanoparticle catalysts.[30] Ni loading slightly decreased the surface area, regardless of La loading. The optimized Ni-La(15)/Al_2O_3 has a specific surface area of 103 m^2/g.

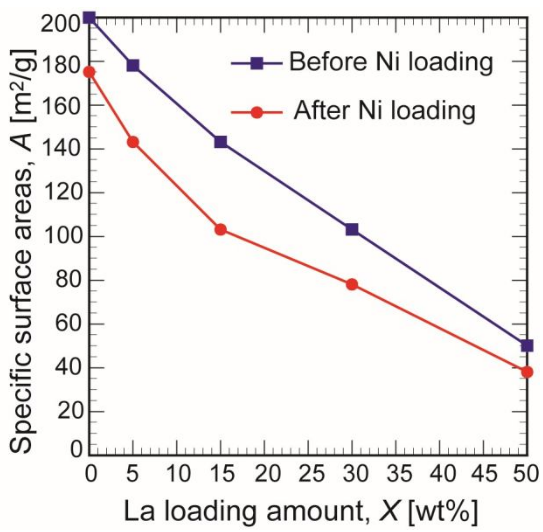

Figure 4. Effect of La loading amount on specific surface area of La(*X*)/Al_2O_3 and Ni-La(*X*)/Al_2O_3.

XRD measurements of Ni-La(*X*)/Al_2O_3 were also performed (Figure 5). The XRD pattern of parent Al_2O_3 showed the diffraction peaks at 2θ = 19.6, 31.9, 37.6, 39.5, 45.8, 60.5, and 66.8°, which are derived from γ-Al_2O_3 (111), (220), (311), (222), (400), (333), and (440), respectively.[34] La loading induced a decrease in the peak intensities owing to their amorphous properties whereas clear diffraction peaks corresponding to La and/or Ni compounds were not observed. These observations are consistent with previously reported results for La-loaded Al_2O_3-supported Ni catalysts.[29] When the La loading amount increased from 15 wt% to 30 wt%, a broad peak appeared around 2θ = 29°, which is possibly assigned to La_2O_3 (101) (JCPDS No. 100210), and its intensity increased with the further increase of loading amount to 50 wt%, suggesting the formation of bulk La oxides. In the case of Ni-La(50)/Al_2O_3, small peaks assignable to $La_2O_2CO_3$ (101) and (103) were also observed at 2θ = 22.8 and 30.6°,[35] which also supports the presence of aggregated La species in high La loading materials.

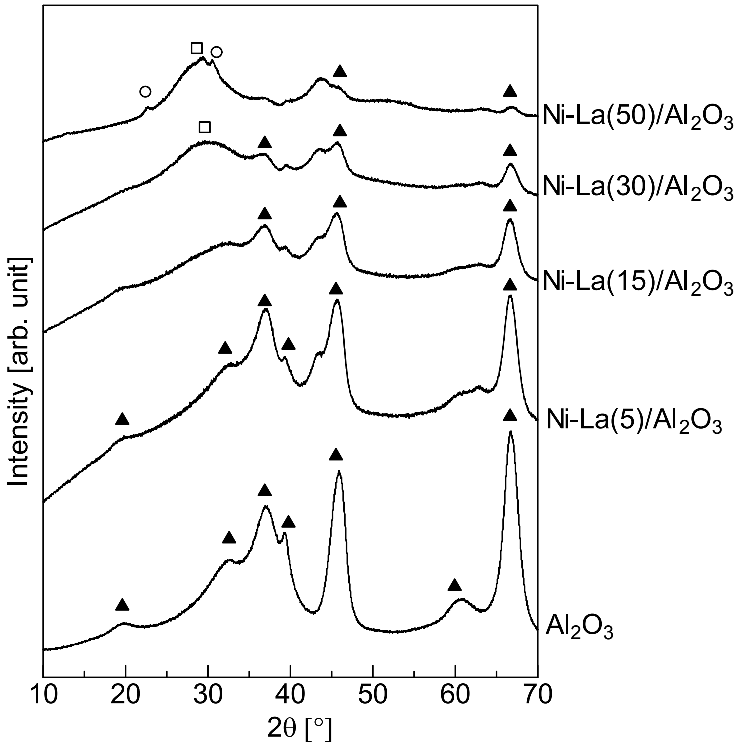

Figure 5 XRD patterns of Al_2O_3 and a series of Ni-La(*X*)/Al_2O_3 (Black triangle: γ-Al_2O_3, Open square: La_2O_3 and/or $La(OH)_3$, Open circle: $La_2O_2CO_3$).

STEM and EDX measurements were performed to investigate the dispersion of the La and Ni species in the optimized Ni-La(15)/Al_2O_3. The aggregation of spherical Al_2O_3 particles of a few dozen nanometers was observed in the HAADF-STEM image (Figure 6). Energy-dispersive X-ray spectroscopy (EDX) mapping showed that La species were highly dispersed over Al_2O_3 while nanosized Ni aggregates were formed. Other results of STEM and EDX are shown in Figure S4 (See the ESI). The average diameter of Ni species was determined as 5.2 nm, as indicated by TEM observation (Figure S5). The presence of La species on the Al_2O_3 surface was supported by ^{27}Al NMR measurements of pure Al_2O_3 and La(15)/Al_2O_3. The NMR spectrum of γ-Al_2O_3 showed the peak at 33 ppm assignable to the penta-coordinated Al^{3+} (Al_V^{3+}), which serve as anchoring sites of loaded metal species, with two major peaks derived from tetracoordinated and hexacoordinated Al^{3+} (Al_{VI}^{3+}) at 70 and 10 ppm, respectively (Figure 7). The La loading significantly decreased the peak intensity of Al_V^{3+} and increased that of Al_{VI}^{3+}. This spectral change was interpreted as an interaction between the co-loaded La species and surface Al_V^{3+} ions.[28] The chemical state of Ni was studied using XAS absorption spectroscopy. The *in-situ* Ni K-edge XANES spectra of Ni-La(15)/Al_2O_3 under H_2 flow at CCR operation temperature were much closer to those of NiO than those of the Ni foil (Figure S6). From the characterization results, highly dispersed La oxide species and nanosized Ni oxides coexist on the Al_2O_3 surfaces.

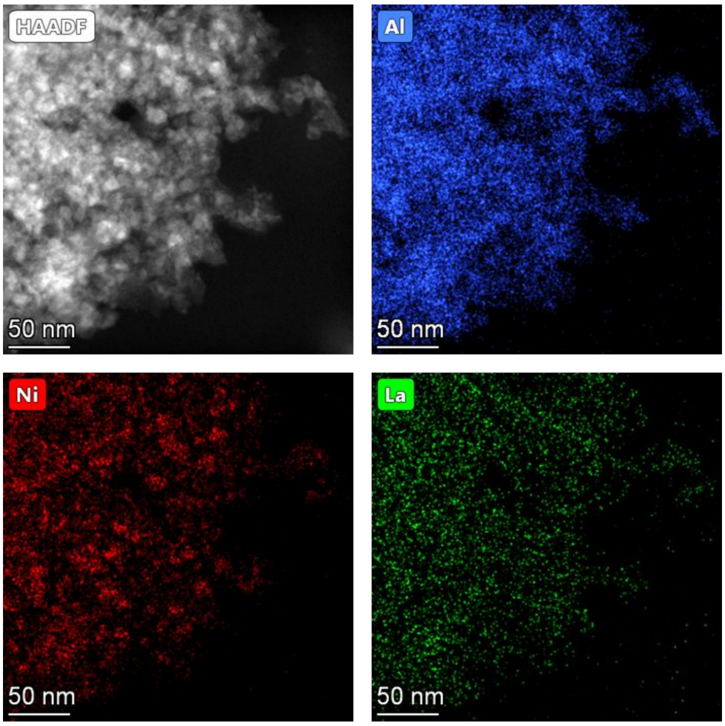

Figure 6 HAADF-STEM image and elemental mapping obtained by EDX spectroscopy for Ni-La(15)/Al_2O_3.

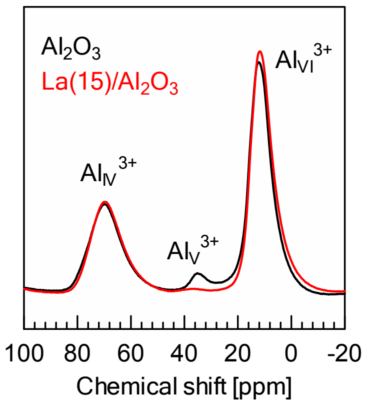

Figure 7 ^{27}Al MAS NMR spectra of Al_2O_3 and La(15)/Al_2O_3.

Effect of La laoding amount on CCR performance

To study how different La loadings affect CCR performance, temperature-programmed surface reaction (TPSR) measurements were performed for CO_2-preadsorbed Ni/Al_2O_3, $Ni-La(15)/Al_2O_3$, and $Ni-La(50)/Al_2O_3$. The CO_2 adsorption was conducted at 100 °C after H_2 reduction, and then the TPSR was performed at a ramping rate of 10 °C /min. Desorbed CO_2 and generated CH_4/CO were continuously monitored using FTIR. The TPSR profiles of a series of $Ni-La(X)/Al_2O_3$ samples are shown in Figure 8a–c. For Ni/Al_2O_3, a weak and broad CH_4 formation peak was observed at ~300–500 °C. By contrast, the TPSR profile of $Ni-La(15)/Al_2O_3$ exhibited a sharp CH_4 formation peak at ~200–400 °C with a CO_2 desorption peak in a lower temperature range (100–250 °C). When $Ni-La(50)/Al_2O_3$ was used for TPSR, the CH_4 formation peak shifted toward a higher temperature region (200–600 °C), although the CO_2 desorption peak almost disappeared. The maximum concentration of generated CH_4 in the lower temperature range of 200–400 °C was lower than that for $Ni-La(15)/Al_2O_3$. The TPSR results implied that the co-loaded La species served as CO_2 adsorption sites, while the reactivity of the captured CO_2 species differed between $Ni-La(15)/Al_2O_3$ and $Ni-La(50)/Al_2O_3$. The temperature-programmed desorption of CO_2 was also investigated for $Ni-La(15)/Al_2O_3$ under similar conditions, except for the gas flow (increasing the temperature under N_2 flow instead of H_2/N_2). The second CO_2 desorption peak was observed at ~400–600 °C (Figure S7). This temperature range is much higher than that for CH_4 formation in the TPSR over $Ni-La(15)/Al_2O_3$. Combined with the results of the XRD measurements, the dispersed La species provided effective CO_2 capture sites for the CCR at lower temperatures.

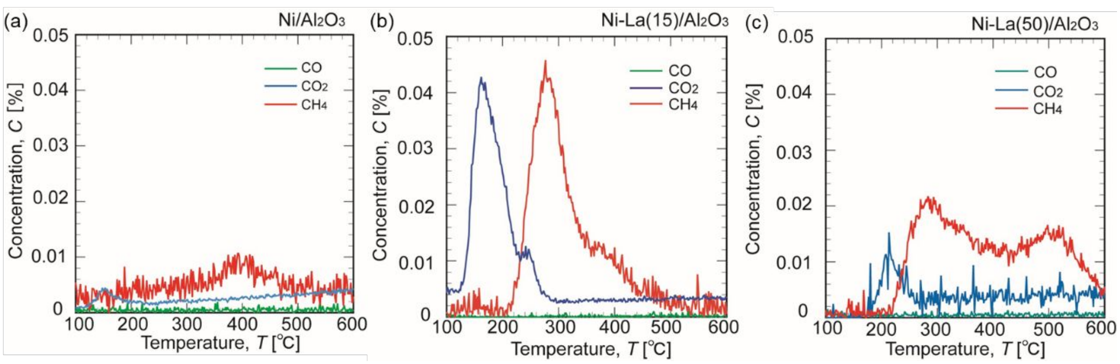

Figure 8 TPSR profiles of CO_2-preadsorbed (a) Ni/Al_2O_3, (b) $Ni-La(15)/Al_2O_3$, and (c) $Ni-La(50)/Al_2O_3$. The H_2 prereduced DFMs were exposed to 1% CO_2+20% O_2/N_2 flow at 100 °C, followed by N_2 purge for 15 min and successive TPSR measurement under 20% H_2/N_2 flow

with increasing the temperature to 600 °C (10 °C/min).

Furtheremore, to investigate the effect of different La loadings on the hydrogenation activity, steady-state CO_2 hydrogenation was also conducted using the above three DFMs. To avoid the reaction of H_2 with O_2, O_2-free condition (1% CO_2+20% H_2/N_2) were used. The concentrations of unreacted CO_2 and generated CH_4 and CO were monitored using FTIR with continuously ramping the temperature at 10 °C/min. In all the cases, CH_4 formation was observed below 200 °C while the temperature at 50% conversion (denoted as $T_{0.5}$) was much lower for La co-loaded DFMs (227 and 240 °C for Ni-La(15)/Al_2O_3 and Ni-La(50)/Al_2O_3, respectively) than for unmodified Ni/Al_2O_3 (294 C) (Figure 9a-c). La co-loading enhanced the catalytic activity of Al_2O_3-supported Ni species for CO_2 methanation, regardless of La loading, which is consistent with the results of a previous study.[29] Combined with the results of CO_2 TPSR, we conclude that the 15 wt% La loading is the most effective because of the formation of a suitable CO_2 capturing ability for CCR at low temperatures rather than the enhancement of the catalytic activity of Ni for CO_2 methanation.

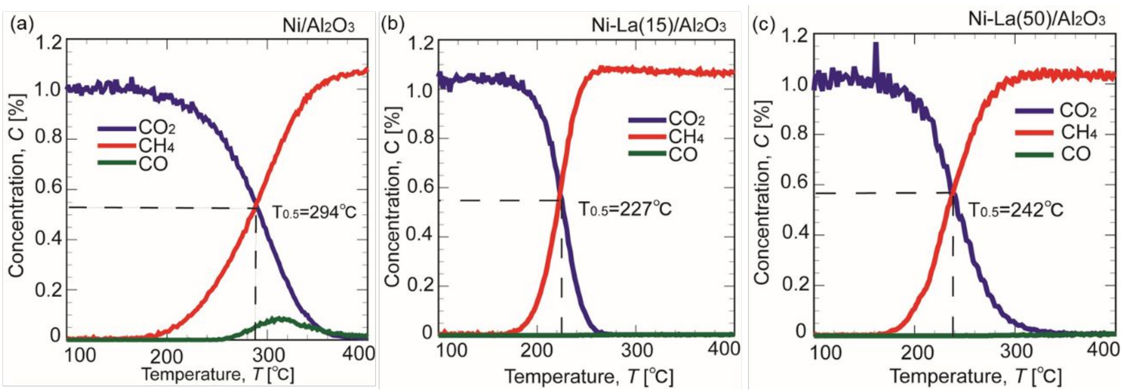

Figure 9. Steady-state CO_2 hydrogenation using (a) Ni/Al_2O_3, (b) Ni-La(15)/Al_2O_3, and (c) Ni-La(50)/Al_2O_3 under O_2-free conditions. In 100 mL/min of 1% CO_2+20% H_2/N_2 flow, the reaction temperature was increased from 100 to 600 °C (10 °C/min) with continuous monitoring of the outlet gas of the reactor using FTIR.

Applicability to direct air capture and methanation

One possible application of CCR over DFMs is the use of DAC and subsequent hydrogenation. Kuramoto et al. studied the CCR of a simulated gas containing ultralow concentrations of CO_2 (400 ppm) over Ni-Na DFMs.[21] Recently, Shimizu and Fujikawa developed a combined system consisting of a membrane-based DAC and a CCR system in which the enriched CO_2 from ambient air by m-DAC (~400–2500 ppm) was successively hydrogenated to CH_4 over Ni-Ca DFMs.[36] Farrauto et al. synthesized a wash-coated monolith of Ru-Na DFMs and investigated the DAC from ambient air (ambient DAC) and methanation.[37] Although considerable effort was devoted to the development of DFMs, the applicability of DAC is still limited.

In this study, we performed ambient DAC and methanation on the developed Ni-La(15)/Al_2O_3. 500 mL/min of compressed air (without dehumidification) was flowed into the reactor containing 2 of Ni-La(15)/Al_2O_3 for 3 min, and then the captured CO_2 air was hydrogenated by switching the gas flow to 100 mL/min of 100% H_2 for 3 min. The ambient DAC and hydrogenation were repeated for 80 cycles. Note that 500 mL/min of N_2 was flowed before gas switching to purge the remaining gas. The concentration profile of CO_2 and CH_4 in the effluent gas is shown in Figure S8. The formation amount was approximately 0.0150 mmol/g whereas maximum concentration of CH_4 reached to approximately 1.1% (Figure 10). By decreasing the flow rate and increasing the DFM amount, the generated CH_4 was enriched. The average CH_4 formation amount in one cycle (0.0292 mmol, corresponding to 0.0146 mmol/g) corresponded more than 90% of the expected CO_2 amount included in 0.5 L/min of air (approximately 500 ppm of CO_2) for 3 min, indicating that almost of CO_2 in air was successfully captured and converted to CH_4. The comparison of CO_2 concentration profile with blank test was also supported the above consideration (Figure S8). Note that the kinetic curve of CO_2 concentration in DAC and methanation was low responsibleness because of the relatively large volume of chamber. The formation amount and maximum concentration of CH_4 were maintained for at least 80 cycles (Figure 10), demonstrating that the good durability of Ni-La(15)/Al_2O_3. The Ni-La(15)/Al_2O_3 after DAC and methanation was characterized by XRD and TEM observation where the XRD pattern and average diameter of Ni species were maintained (Figure S5 and S9). There results were consistent with the good durability of Ni-La(15)/Al_2O_3. Regarding the effect of humidity, we conducted the CCR experiments using simulated CO_2 gas with or without cofeeding of vapor (100 RH%

at 25 °C) (Figure S10). The co-feeding of vapor resulted in the decrease of the formation amount and maximum concentration of CH_4 (Table S3). Our results demonstrate the potential of CCR for the capture and direct utilization of CO_2 in ambient air to produce enriched CH_4 while dehumidification is necessary for application under realistic conditions.

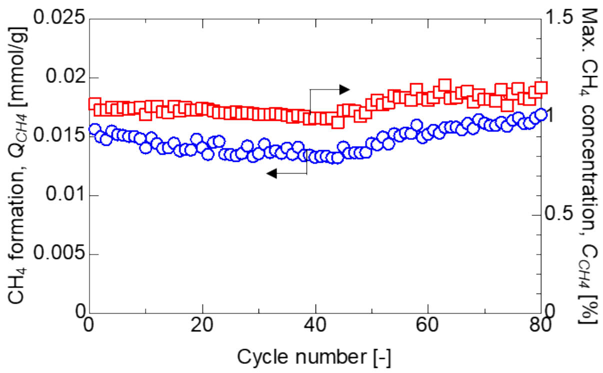

Figure 10. CH_4 formation amount (Q_{CH4}) and C_{Max} in ambient DAC and methanation for 80 cycles. The concentration profile of CO_2 and CH_4 is shown in Figure S8.

Conclusion

In conclusion, we developed Ni and La co-loaded Al_2O_3, Ni-La/Al_2O_3, as Ni-based DFMs for CO_2 capture from a mixture of O_2 and selective hydrogenation CH_4. The Ni-La/Al_2O_3 exhibited 98% selectivity to CH_4 formation, which is higher than those obtained using Ni/Al_2O, Ni-Na, and Ni-Ca/Al_2O_3 at relatively mild conditions using atmospheric H_2 pressure at 350 °C. The effect of the La loading amount on CCR performance was also studied. The optimal La loading amount was 15 wt%, whereas increasing the La loading amount to 50 wt% drastically decreased the amount formed and maximum concentration of CH_4. The combined results of XRD, TPSR, and TPD experiments revealed that highly dispersed La species serve as effective CO_2 capture sites for CCR under the isothermal conditions of 350 °C. The co-loaded La species improved the CH_4 selectivity regardless of the La loading amount, as indicated by the steady-state CO_2 hydrogenation test. Finally, ambient DAC for methanation was demonstrated using the developed Ni-La/Al_2O_3 DFMs, where the CCR performance was maintained for at least 80 cycles. The co-feeding of vapor in simulated CO_2 gas decreased CCR performance, implying the necessity of dehumidification for application under realistic conditions.

Author contributions

Z.M. conceptualized and supervised this work. T.T. performed the most of experimental investigations and conducted the data analyses. R.O. and H.H. performed the sample preparation, performed NMR experiments, and data analysis. T.T. and Z.M. co-wrote the draft, and Z.M. and N.N. modified the manuscript. Finally, all the authors approved the final manuscript.

Conflicts of interest

There are no conflicts to declare.

Acknowledgements

This study was is based on results obtained from a project, JPNP20004, subsidized by the New Energy and Industrial Technology Development Organization (NEDO). A part of this study was financially supported by the JST, PRESTO Grant Number JPMJPR22Q7, and by KAKENHI (Grant Nos. JP23H01765) from the Japan Society for the Promotion of Science (JSPS). Z. M. thanks a JACI Prize for Encouraging Young Researcher and the Iwatani Naoji Foundation. N_2 adsorption experiments were performed by Dr. Shuhei Shimoda at Hokkaido University, supported by the Joint Usage/Research Center for Catalysis. HADDF-STEM and EDX measurements were conducted by Dr. Ryo Ota at the Hokkaido University, supported by "Nanotechnology Platform Program" of MEXT (Proposal No. JPMXP09A21HK0027). We thank Dr. Koji Yazawa, Dr. Shinobu Ohki, and Dr. Kenzo Deguchi for NMR experiments. NMR experiments were supported by "Advanced Research Infrastructure for Materials and Nanotechnology in Japan (ARIM)" of MEXT (Proposal No. JPMXP1223NM0075). We also acknowledge Dr. Takashi Toyao and Mr. Duotian Chen for XAS measurement performed at BL14B2 of SPring-8 (Proposal No. 2023A1931) and Dr. Shiro Seki and Mr. Koji Hiraoka for XRD analysis.

References

1 M. T. Ho, G. W. Allinson and D. E. Wiley, *Ind. Eng. Chem. Res.*, 2008, **47**, 4883–4890.

2 H. A. Patel, J. Byun and C. T. Yavuz, *ChemSusChem*, 2017, **10**, 1303–1317.

3 K. T. Leperi, D. Yancy-Caballero, R. Q. Snurr and F. You, *Ind. Eng. Chem. Res*, 2019, **58**, 18241–18252.

4 M. T. Dunstan, F. Donat, A. H. Bork, C. P. Grey and C. R. Müller, *Chem. Rev.*, 2021,

121, 12681–12745.

5 A. Samanta, A. Zhao, G. K. H. Shimizu, P. Sarkar and R. Gupta, *Ind. Eng. Chem. Res.*, 2012, **51**, 1438–1463.

6 X. Zhu, W. Xie, J. Wu, Y. Miao, C. Xiang, C. Chen, B. Ge, Z. Gan, F. Yang, M. Zhang, D. O'Hare, J. Li, T. Ge and R. Wang, *Chem. Soc. Rev.*, 2022, **51**, 6574–6651.

7 F. Marocco Stuardi, F. MacPherson and J. Leclaire, *Curr Opin Green Sustain. Chem*, 2019, **16**, 71–76.

8 J. Chen, Y. Xu, P. Liao, H. Wang and H. Zhou, *Carbon Capture Science & Technology*, 2022, **4**, 100052.

9 I. S. Omodolor, H. O. Otor, J. A. Andonegui, B. J. Allen and A. C. Alba-Rubio, *Ind. Eng. Chem. Res.*, 2020, **59**, 17612–17631.

10 M. Abdallah, Y. (Iris) Lin and R. Farrauto, *Appl Catal B*, 2023, **339**, 123105.

11 C. Jeong-Potter and R. Farrauto, *Appl. Catal. B*, 2021, **282**, 119416.

12 M. S. Duyar, S. Wang, M. A. Arellano-Treviño and R. J. Farrauto, *Journal of CO_2 Utilization*, 2016, **15**, 65–71.

13 C. Jeong-Potter, M. Abdallah, C. Sanderson, M. Goldman, R. Gupta and R. Farrauto, *Appl. Catal. B*, 2022, **307**, 120990.

14 M. A. Arellano-Treviño, N. Kanani, C. W. Jeong-Potter and R. J. Farrauto, *Chem. Eng. J.*, 2019, **375**, 121953.

15 M. S. Duyar, M. A. A. Treviño and R. J. Farrauto, *Appl. Catal. B*, 2015, **168–169**, 370–376.

16 L. Li, S. Miyazaki, S. Yasumura, K. W. Ting, T. Toyao, Z. Maeno and K. Shimizu, *ACS Catal.*, 2022, **12**, 2639–2650.

17 Z. Boukha, A. Bermejo-López, U. De-La-Torre and J. R. González-Velasco, *Appl. Catal. B*, 2023, **338**, 122989.

18 L. C. Wirner, F. Kosaka, T. Sasayama, Y. Liu, A. Urakawa and K. Kuramoto, *Chem. Eng. J.*, 2023, **470**, 144227.

19 D. Pinto, S. Minorello, Z. Zhou and A. Urakawa, *J. Environment Sci.*, DOI: 10.1016/j.jes.2023.06.006.

20 J. Lee and J. Otomo, *Ind. Eng. Chem. Res.*, 2023, **62**, 12096–12108.

21 F. Kosaka, Y. Liu, S.-Y. Chen, T. Mochizuki, H. Takagi, A. Urakawa and K. Kuramoto, *ACS Sustain. Chem. Eng.*, 2021, **9**, 3452–3463.

22 T. Hyakutake, W. van Beek and A. Urakawa, *J. Mater. Chem. A*, 2016, **4**, 6878–6885.

23 M. A. Arellano-Treviño, Z. He, M. C. Libby and R. J. Farrauto, *J. CO_2 Utilization*, 2019, **31**, 143–151.

24 L. Hu and A. Urakawa, *Journal of CO2 Utilization*, 2018, **25**, 323–329.

25 L. F. Bobadilla, J. M. Riesco-García, G. Penelás-Pérez and A. Urakawa, *J. CO_2 Utilization*, 2016, **14**, 106–111.

26 A. Bermejo-López, B. Pereda-Ayo, J. A. González-Marcos and J. R. González-Velasco, *J. CO_2 Utilization*, 2019, **34**, 576–587.

27 E. García-Bordejé, A. Belén Dongil, J. M. Conesa, A. Guerrero-Ruiz and I. Rodríguez-Ramos, *Chem. Eng. J.*, 2023, **472**, 144953.

28 J. H. Kwak, J. Hu, A. Lukaski, D. H. Kim, J. Szanyi and C. H. F. Peden, *J. Phys. Chem. C*, 2008, **112**, 9486–9492.

29 G. Garbarino, C. Wang, T. Cavattoni, E. Finocchio, P. Riani, M. Flytzani-Stephanopoulos and G. Busca, *Appl. Catal. B*, 2019, **248**, 286–297.

30 Y. Jing, Z. Cai, C. Liu, T. Toyao, Z. Maeno, H. Asakura, S. Hiwasa, S. Nagaoka, H. Kondoh and K. Shimizu, *ACS Catal.*, 2020, **10**, 1010–1023.

31 H. Muraki, H. Shinjoh and Y. Fujitani, *Appl Catal*, 1986, **22**, 325–335.

32 T. Zhang, H. Ai and Q. Liu, *Ener. Tech.*, 2019, **7**, 1900531.

33 B. Ravel and M. Newville, *J Synchrotron Radiat*, 2005, **12**, 537–541.

34 R. Prins, *J. Catal.*, 2020, **392**, 336–346.

35 Y. Dai, M. Xu, Q. Wang, R. Huang, Y. Jin, B. Bian, C. Tumurbaatar, B. Ishtsog, T. Bold and Y. Yang, *Appl. Catal. B*, 2020, **277**, 119271.

36 L. Li, S. Miyazaki, Z. Wu, T. Toyao, R. Selyanchyn, Z. Maeno, S. Fujikawa and K. Shimizu, *Appl. Catal. B*, 2023, **339**, 123151.

37 M. Abdallah, Y. (Iris) Lin and R. Farrauto, *Appl. Catal. B*, 2023, **339**, 123105.

The data that support the findings of this study are available from the corresponding author, Z.M., upon reasonable request.